Journal of Magnetism and Magnetic Materials 545 (2022) 168772

Contents lists available at ScienceDirect

Journal of Magnetism and Magnetic Materials

journal homepage: www.elsevier.com/locate/jmmm

Structural and magnetic characterisation of a biocompatible magnetic nanoparticle assembly

Vilmos Vékony [a,*], Csaba Matta [c], Petra Pál [b], István A. Szabó [a]

[a] Department of Solid State Physics, Faculty of Science and Technology, University of Debrecen, Bem tér 18/b, Debrecen H-4039, Hungary
[b] Department of Experimental Physics, Faculty of Science and Technology, University of Debrecen, Bem tér 18/b, Debrecena H-4039, Hungary
[c] Department of Anatomy, Histology and Embryology, Faculty of Medicine, University of Debrecen, Nagyerdei krt 98, Debrecen H-4032, Hungary

ARTICLE INFO

Keywords:
Magnetic nanoparticle
Raman spectroscopy
MFM
TEM
VSM

ABSTRACT

Magnetic nanoparticles have several promising biomedical applications. One example is the magnetic nanoparticle-based hyperthermia, where the magnetic nanoparticles absorbed by the tumor cells are subjected to alternating magnetic field to generate local heating. Other applications rely on the effect of static magnetic fields to collect or rearrange cells, which are covered with magnetic nanoparticle containing substrates. In both cases, the effect of clustering largely modifies the magnetic properties of these materials. In the present study, we have examined the commercially available multicomponent material, NanoShuttle™-PL (Greiner Bio-One) particles composed of gold, iron oxide and poly-L-lysine, which are used for the creation of levitated 3D cell cultures. While this material is often used for cell culture studies, there is no available data on its magnetic and structural properties. The aim of the study was to understand the magnetic properties of this composite material based on the characterisation of the size distribution and clustering of the magnetic nanoparticles. We have performed RAMAN, AFM/MFM measurements and SEM/STEM investigation of the composite material. Magnetic properties were investigated with a vibrating sample magnetometer (VSM) both in the liquid state and in the surface extracted form.

1. Introduction

Magnetic nanoparticles (MNP) have a large number of applications, including hyperthermia and magnetic levitation of 3D cell cultures.

In the case of hyperthermia these nanoparticle systems are capable of transferring energy to their environment from an alternating magnetic field, which is suitable for the treatment of cancer [1]. Relatively small tumors (3–6 cm) are treated with local hyperthermia procedures [2]. Heat loss can result from three processes: Resistance heating due to the eddy currents, magnetic heating due to the hysteresis loss of multidomain nanoparticles and magnetic heating due to the Brownian and Néel relaxation processes. Its advantage over other methods is that the heat generation is local so that it destroys the tumor cells directly. The aim of the hyperthermia research is the maximization of the dissipated energy. The frequency range used for tumor therapy treatments is between 0.05 and 1.2 MHz, and the applied field strength is 0–5 kA/m.

In the case of magnetic levitation, 3D tissue growth occurs by placing cells containing magnetic nanoparticles in a spatially varying external magnetic field. The growth will be in the formed clusters [3]. This application is suitable for example for the modelling of 3D cancer growth [4]. In this case the magnetic particles can be moved with the external magnetic field to different positions within the body or can be easily collected from a solution. One can also combine the two cases for more localized hyperthermia treatment [5].

The most commonly used MNP materials are the iron oxide nanoparticles [6–8]. One of the most popular and simplest method of preparation is the continuous precipitation of iron nanoparticles in the aqueous phase in the presence of surfactants. It is often necessary to modify the surface of nanoparticles without changing the bulk properties. Reasons for this include, for example, changing the surface composition, blood and biocompatibility and protection. Several methods are known for surface modification, such as surface adsorption of surfactants and polymers, high-energy radiation and covalent binding of desired ligand onto surface functional groups via different activation methods [9].

Development of biocompatible nanoparticles is a long process, so we have studied the commercially available NanoShuttle™-PL liquid in this study, which will be used in cell culture studies later on. This is a

* Corresponding author.
E-mail address: vekony.vilmos@science.unideb.hu (V. Vékony).

https://doi.org/10.1016/j.jmmm.2021.168772
Received 17 June 2021; Received in revised form 29 October 2021; Accepted 4 November 2021
Available online 9 November 2021

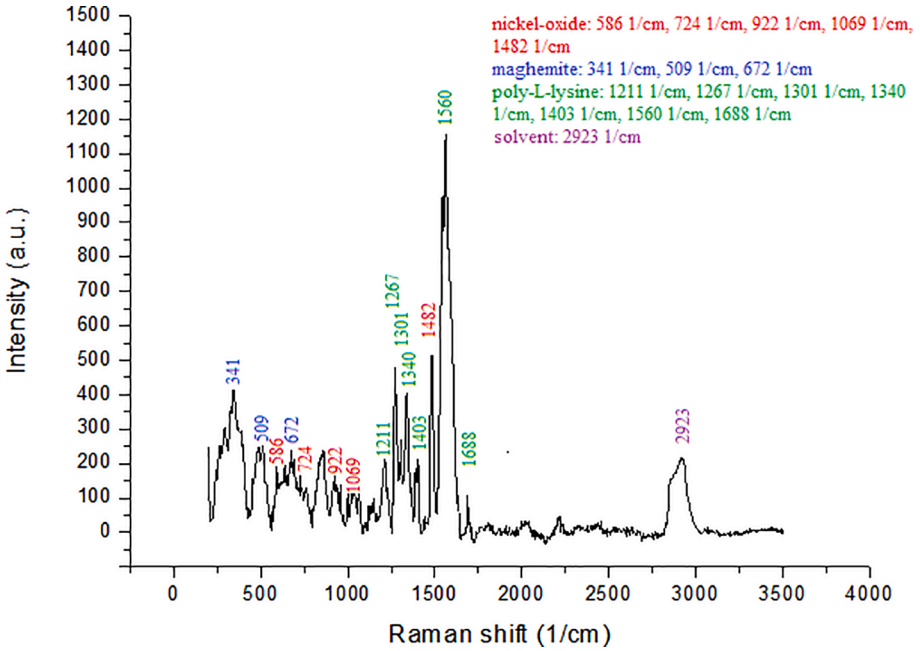

Fig.1. Raman spectrum of the sample. Three ingredients have been identified: nickel-oxide, maghemite and poly-L-lysine. The 2923 1/cm is the solvent peak and belongs to the C–H stretching region.

nanoparticle assembly consisting of gold, iron oxide, and poly-L-lysine. The poly-L-lysine will non-specifically bind to cell membranes via electrostatic interactions.

The NanoShuttle™-PL material is often used for the creation of free-floating cell cultures. To our knowledge the structure and the magnetic properties were not presented in the literature for this material. This can be important in relation to the cell culture studies which we are planning to perform. On the other hand, this material would be appropriate for our hyperthermic experimental research. As mentioned above, the NanoShuttle™-PL contains gold nanoparticles which are able to absorb near-infrared light [10]. This can also be used to warm tumors. In addition, they are able to absorb a large amount of X-rays. Concentrated radiation absorption is then seen in the tumor. In addition, the clustering behavior of ferromagnetic particles can have a positive effect on energy loss [11–13]. Higher heat generation is observed in chain-shaped structures [14]. Thus, the use of these nanoparticles results a better combination of radiotherapy and hyperthermia. From the point of view of material science, the magnetic behavior of the clusters of magnetic particle systems is also very active research field both in their theoretical and experimental aspects, and thus the NanoShuttle™-PL liquid can be a good reference material for such studies.

In the present article, we determined the material composition and the particle size distribution of the NanoShuttle™-PL sample, and examined its magnetic properties. These are essential for the physical characterisation of the sample and the latter experimental applications.

2. Experimental

For SEM/STEM and Raman measurements, the sample was prepared as follows. The nanoparticles in the sample were in an oily medium. The carrier was dissolved in alcohol. Mixing was performed by ultrasound equipment. In the process, a magnet held the nanoparticles together. After mixing, the oil precipitated on top of the liquid. This has been removed from the liquid. This process was repeated four times.

The VSM measurements were performed first with the original liquid dispersed sample. For the measurements, the liquid had to be removed to examine the sample in the solid state. This was achieved by localizing the nanoparticles deposited in the sample holder with a permanent magnet and pouring out the liquid. After drying in air for 24 h, the remaining liquid was evaporated.

The Raman spectroscopy and the AFM/MFM measurements were performed with a Horiba LabRam nano instrument. For the MFM measurements “two pass scanning” [15] method was used. Firstly, the tip scans the sample topology in the tapping mode. Secondly the magnetic structure is determined.

Raman spectroscopy has been used to identify chemical and biological molecules by their Raman spectra [16]. With this equipment, the exact material composition can be determined. The alcohol dissolved particles were put a microscope slide and the Raman measurements were performed on different clusters located under the optical microscope. During the work, 633 nm laser was used as excitation source and the measurement time was 30 s. The excitation beam was focused onto the sample surface with a 50x lens. The beam intensity was 0.21 mW which is 3.2% of the maximum intensity.

The microstructure and composition of the sample was studied by a Thermo Fisher Scientific-scios 2 instrument SEM and STEM microscope. This instrument was supplemented with energy-dispersive x-ray spectroscopy (EDX) to provide information on the spatial distribution in an area of the material.

The magnetization curves were recorded with a home-built vibrating sample magnetometer (VSM) [17]. With this instrument, the magnetization curves of the sample can be recorded. An electromagnetic vibration system provides sinusoidal motion to the sample. The sample performs this motion in the magnetic field produced by the excitation coils. As a result, a voltage is induced in a measuring coil, from which the magnetic moment of the sample can be determined.

3. Results and discussions

3.1. Raman spectroscopy

The Raman spectrum (Fig.1) shows that the sample contains poly-L-lysine and iron-oxide as reported by the manufacturer. The iron-oxide is in maghemite form, there are many peaks. Surprisingly, also nickel-oxide was identified. The gold has no Raman activity because of crystal symmetry. The peaks at 2018 1/cm and 2225 1/ cm are not true peaks but indicate background. The 2923 1/cm is the solvent peak and belongs to the C–H stretching region (2800–3100 1/cm) [18].

Table 1
Observed Raman shifts and peak intensities of the different materials.

Material	Raman shift (1/cm)	Peak intensity (a.u.)
nickel-oxide	586, 724, 922, 1069, 1482	195, 177, 159, 104, 538
maghemite	341, 509, 672	418, 250, 236
poly-L-lysine	1211, 1267, 1301, 1340, 1403, 1560, 1688	211, 500, 272, 418, 222, 1200, 113
solvent	2923	220

The following peaks (Table 1) were identified based on the literature. The numbers in parenthesis are the literature data.

The **nickel-oxide (red)** peaks are the follows [19–21]: one phonon excitation: 586 1/cm (560) (1 longitudinal phonon mode); two phonon excitations: 724 1/cm (740) (2 transversal optical phonon modes), 922 1/cm (925) (1 transversal optical and 1 longitudinal optical phonon modes), 1069 1/cm (1100) (2 longitudinal optical phonon modes); two magnon band: 1482 1/cm (1500).

Based on [22–24] our sample contains **maghemite (blue)**. The maghemite peaks: 341 1/cm (365, 350, 350), 509 1/cm (511, 512, 500), 672 1/cm (700, 665, 700) (longitudinal optical mode). There are many peaks in this part of the spectrum, there is a lot of overlap. As particle size decreases, these lines become broader, shifting towards lower wavenumbers. The wide size distribution is the reason of the difference between the bulk material and our sample.

The **poly-L-lysine (green)** peaks are the follows [25–27]: the AmIII region ($C-N$ strechting coupled with $N-H$ bending): 1211 1/cm (1218) (β-turn), 1267 1/cm (1253/1267, 1245) (α-helix and π-bulge/helix), 1301 1/cm (1296, 1296), 1340 1/cm (1332, 1316), the $C_\alpha-H$ (bending) peak: 1403 1/cm (1395, 1396), the AmII peak ($C-N$ strechting coupled with $N-H$ bending): 1560 1/cm (1560, 1564) and the AmI peak ($C=O$ strechting vibration): 1688 1/cm (1665, 1670).

3.2. SEM, STEM, EDX measurements

During the EDX measurement, the sample was scanned at 1100 nm while providing information on the material composition. Fig. 2 shows that there are 3 metallic materials in the sample. The larger ellipsoidal shape particles are the gold particles. The other two materials are iron and nickel.

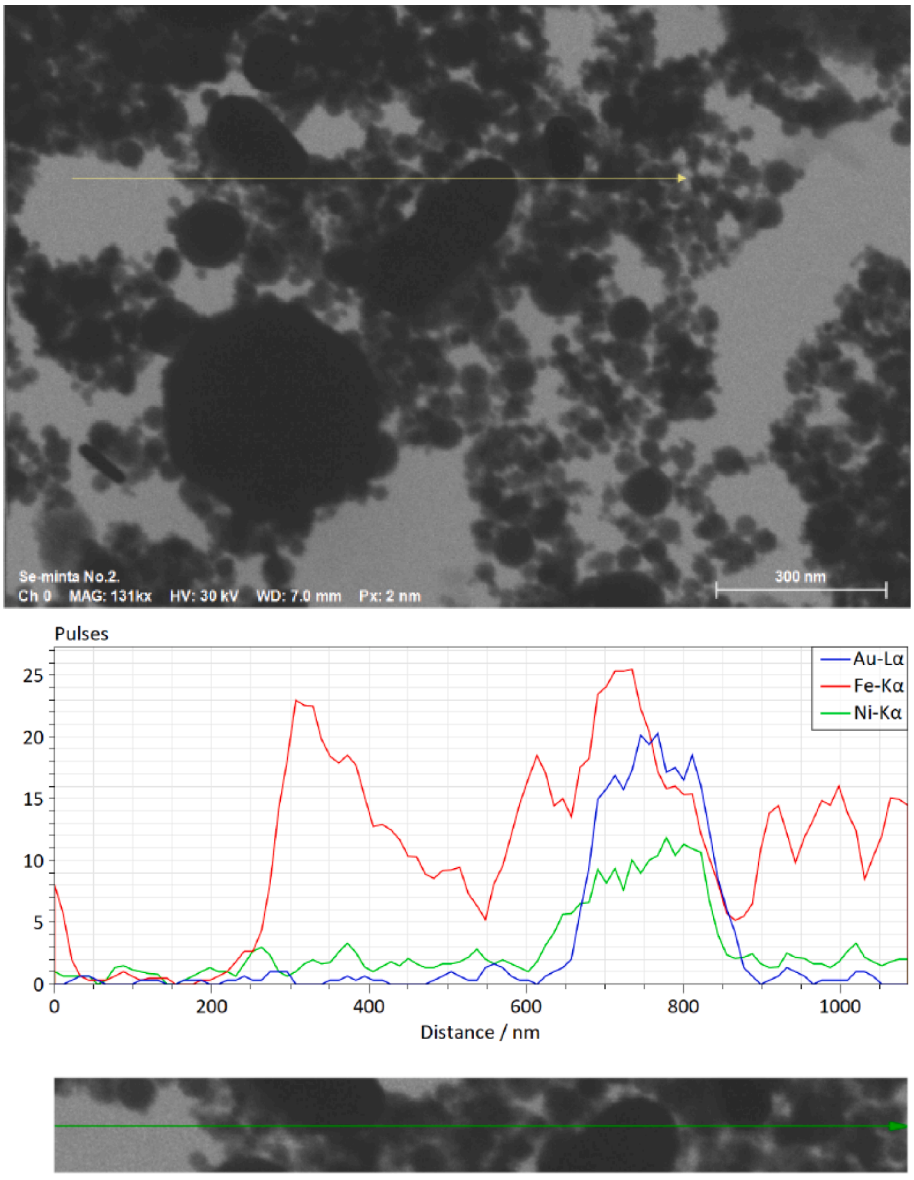

Fig.2. It can be seen above a STEM image of an area of the sample and the scanned line. The magnification of the STEM image is 131000×. The spatial material distribution from the EDX measurement is shown below.

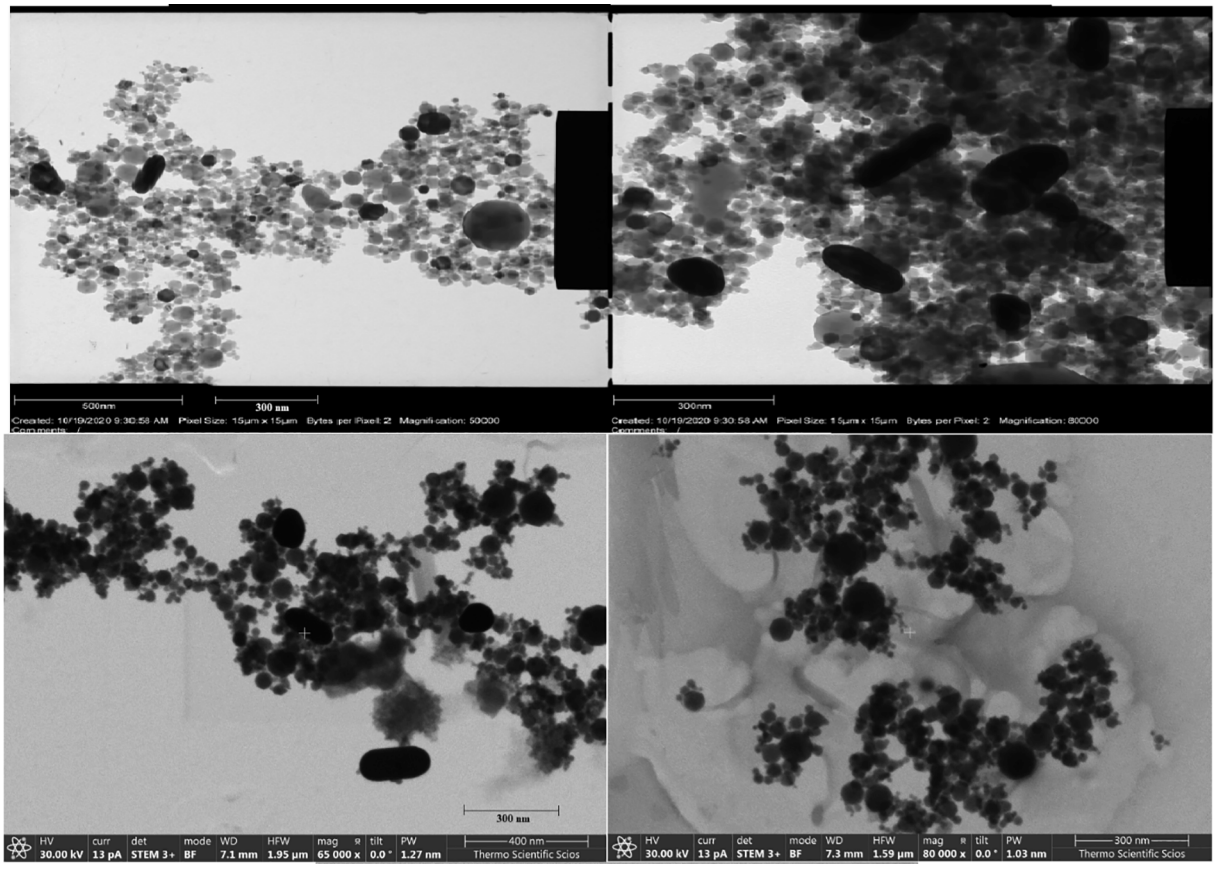

Fig. 3. TEM (top) and STEM (bottom) images of the iron-oxide nanoparticles and gold particles embed in a polymer matrix. The clustering tendency of the magnetic nanoparticles can be clearly seen.

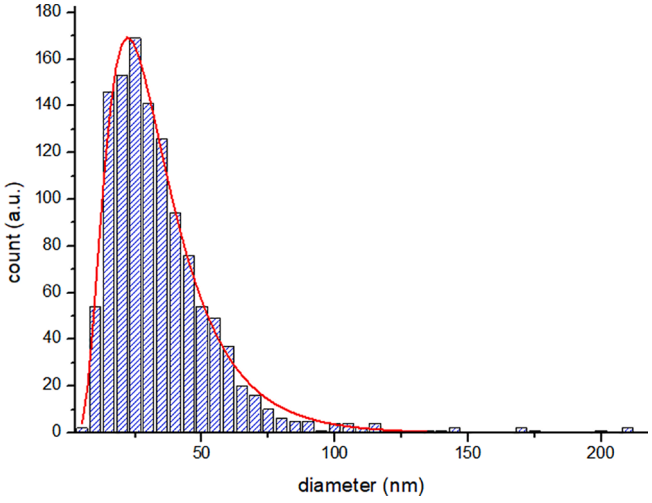

Fig.4. The size distribution of the nanoparticles in the four images (the "box size" is 5 nm). The fitted curve corresponds to the lognormal distribution.

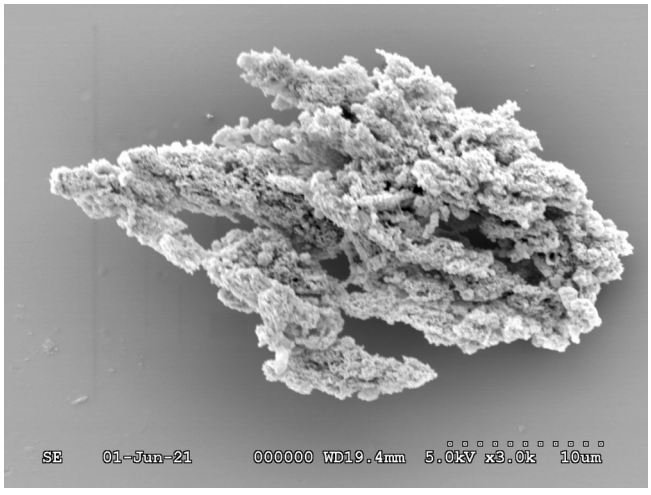

Fig.5. The microstructure of the polymer particles aggregated on the surface of Si under the effect of external magnetic field.

Typical TEM and STEM micrographs of the nanoparticles are presented in Fig. 3. Particle size distribution in NanoShuttle™-PL was estimated from the TEM and STEM image analysis by using the ImageJ and Origin software. The analysis was performed on each image. A large number of particles of different sizes were selected and measured in the ImageJ. The resulting data set was processed in the Origin. Particles were classified in 5 nm increments in the recorded histogram. A curve corresponding to a lognormal distribution was fitted to this.

The histograms of the particle size distribution are presented in Fig. 4. The fitting function was the lognormal distribution:

$$f(d,\mu,\sigma) = \frac{A}{d\sigma\sqrt{2\pi}} e^{-\frac{(\ln d - \ln\mu)^2}{2\sigma^2}}$$

where A is a fitting parameter, d is the diameter, σ and $\ln\mu$ are the standard deviation and the mean of the variable's natural logarithm. We have obtained the following values for these based on the fitting: $A = 6042 \pm 90$, $\sigma = 0.55 \pm 0.01$, $\ln\mu = 3.40 \pm 0.05$. The corresponding average nanoparticle size is $\mu = 30$ nm.

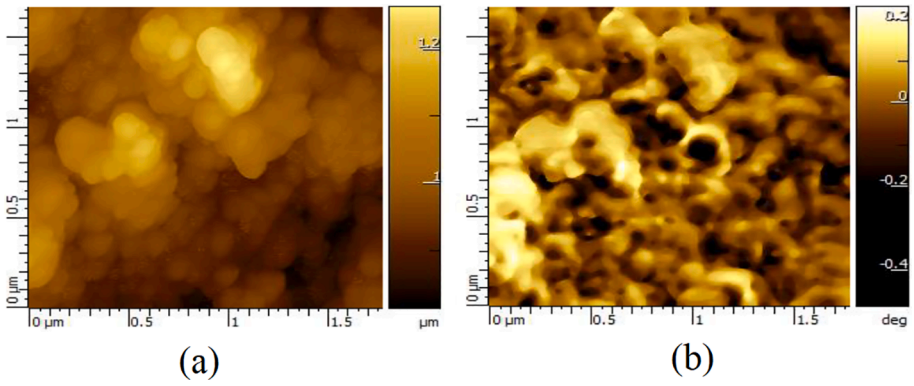

Fig.6. AFM (a) and MFM (b) images of the sample. The clusters and magnetizable regions (100–200 nm) can be seen in the images.

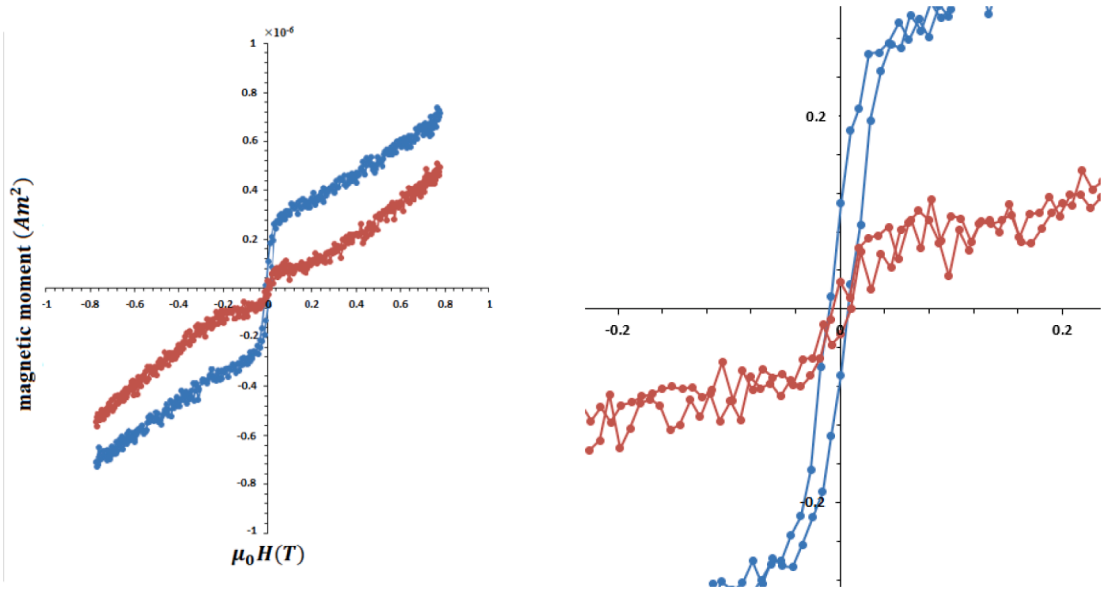

Fig.7. Magnetization curves of the sample in liquid dispersed (blue) and surface extracted (red) state. On the right side the curves are magnified at low external fields.

Based on the electron microscopy observations we can conclude, that the magnetic particles and the gold particles are dispersed in the polymer matrix "flakes". These polymer matrix particles are aggregated in a magnetic field or on the substrate into larger clusters with an open structure (Fig. 5).

3.3. AFM and MFM measurements

The AFM and MFM images are shown in the Fig. 6. There is a clear correspondence for some particles on the topographic image and the magnetic information of the lift-mode phase shift image. Dark contrast means attraction, white contrast close to a dark contrast means repulsion. The AFM topography has a lower resolution than the STEM images, so it is difficult to identify the different components. On the MFM image one can see the presence of the magnetic particles and clusters. The image analysis was also performed on the MFM image, which showed that the size of magnetizable (dark) regions are around 100–200 nm.

3.4. VSM measurements

Static magnetization curves were recorded in a vibrating sample magnetometer for two different states of the nanoparticles: liquid dispersed state and surface extracted. The VSM measurements of clustered MNPs were carried out at 300 K in the applied magnetic field sweeping from −0,8 to 0,8 T. Due to the small amount of sample, it was not possible to measure masses with sufficient accuracy. Therefore, instead of magnetization, the magnetic moment was measured (the sample holder signal was removed from the sample signal). The sample have smaller magnetic moment in the surface extracted state, than the liquid dispersed state, because less nanoparticles are in the surface extracted state.

The nearly linear magnetization shows high coercivity resulting from particle clustering of the nanoparticles as shown on Fig. 7. a. The clustering effects was studied in detail in the literature [28] in FeraSpin TM -R, which contains dense clusters of iron oxide magnetic nanoparticles by P Bender at al. Our magnetization curves show similar tendencies. At low external fields there is a short horizontal part which is followed by a continuous rise of the magnetization curve. The saturation level was not reached in our case because of the lower maximal field value. This behavior is thus in accordance with the effect of clustering.

We have also observed an additional contribution with hysteresis at low excitation field especially in the liquid state shown on Fig. 7. b. A large part of the maghemite particles are above the limit of superparamagnetic range 30 nm [29], thus the presence of a small hysteresis is expected. As the nanoparticles are embedded in the polymer matrix, they cannot reorient themselves individually. In the liquid dissolved phase, the whole polymer flakes can rotate, which can have an additional component in the magnetization curve. In liquid dispersed state it

is possible to reorient the large clusters in the presence of external magnetic field, while in surface extracted state this cannot occur. This requires further microscopic investigation in situ. If present, this can be used for the manipulation of cell cultures in contact with the magnetic clusters with low external fields. The apparent susceptibility, which is the slope of the magnetization curve is nearly the same for the surface extracted and the free-floating states. This can be related to the gradual reorientation of the magnetic moments of the magnetic particles with different sizes and thus different shape anisotropy factors and magnetic moments under the influence of the external field and the neighboring particles magnetic fields.

4. Conclusions

We analyzed the magnetic properties and microstructure of a commercial sample NanoShuttle™-PL. From the Raman measurements we identified the main chemical components. The STEM/SEM measurements was used to determine the size distribution of the nanoparticles. The clustering tendencies could be observed on the STEM/SEM images, that the nanoparticles were forming chains and clusters of chains which are embedded in a matrix together with gold nanoparticles. The VSM measurements have shown that there is an additional contribution when the clusters can be reoriented in the fluid phase. The AFM/MFM examination also revealed the presence and distribution of magnetizable components on the microscale. The measured macroscopic magnetic properties and the microscopic observation of the cluster structure and local magnetization properties can be used to develop more complex cell manipulation techniques in the future.

Declaration of Competing Interest

The authors declare that they have no known competing financial interests or personal relationships that could have appeared to influence the work reported in this paper.

Acknowledgement

This work was financially supported by the grant GINOP-2.3.2-15-2016-00041. The project is co-financed by the European Unionand the European Regional Development Fund. The support of the ED_18-1-2019-0028 Thematic Excellence Program is gratefully acknowledged.

References

[1] D. Ortega, Q.A. Pankhurst, Magnetic hyperthermia, Nanoscience 1 (2013) 60–88, https://doi.org/10.1039/9781849734844-00060.
[2] Z. Behrouzkia, Z. Joveini, B. Keshavarzi, N. Eyvazzadeh, R.Z. Aghdam, Reza Zohdi Aghdam, Hyperthermia: how can it be used? Oman Med. J. 31 (2) (2016) 89–97, https://doi.org/10.5001/omj.2016.19.
[3] W.L. Haisler, D.M. Timm, J.A. Gage, H. Tseng, T.C. Killian, G.R. Souza, Three-dimensional cell culturing by magnetic levitation, Nat. Protocols 8 (10) (2013) 1940–1949, https://doi.org/10.1038/nprot.2013.125.
[4] H. Jaganathan, J. Gage, F. Leonard, S. Srinivasan, G.R. Souza, B. Dave, B. Godin, Three-dimensional in vitro co-culture model of breast tumor using magnetic levitation, Sci. Rep. 4 (2014) 6468, https://doi.org/10.1038/srep06468.
[5] S. Libring, Á. Enríquez, H. Lee, and L. Solorio, In VitroMagnetic Techniques for Investigating Cancer Progression, Cancers 2021, 13, 4440. (2021) https://doi.org/10.3390/cancers13174440.
[6] C. Baker, S. Ismat Shah, S.K. Hasanain, Magnetic behavior of iron and iron-oxide nanoparticle/polymer composites, J. Magn. Magn. Mater. 280 (2-3) (2004) 412–418, https://doi.org/10.1016/j.jmmm.2004.03.037.
[7] S. Kralj, D. Makovec, Magnetic assembly of superparamagnetic iron oxide nanoparticle clusters into nanochains and nanobundles, ACS Nano 9 (10) (2015) 9700–9707, https://doi.org/10.1021/acsnano.5b02328.
[8] J. Carvell, E. Ayieta, A. Gavrin, R. Cheng, V.R. Shah, P. Sokol, Magnetic properties of iron nanoparticle, J. Appl. Phys. 107 (10) (2010) 103913, https://doi.org/10.1063/1.3428415.
[9] N.M. Mahmoodi, Surface modification of magnetic nanoparticle and dye removal from ternary systems, J. Ind. Eng. Chem. 27 (2015) 251–259, https://doi.org/10.1016/j.jiec.2014.12.042.
[10] J.F. Hainfeld, L. Lin, D.N. Slatkin, F.A. Dilmanian, T.M. Vadas, H.M. Smilowitz, Gold nanoparticle hyperthermia reduces radiotherapy dose, nanomedicine: nanotechnology, Biol. Med. 10 (8) (2014) 1609–1617, https://doi.org/10.1016/j.nano.2014.05.006.
[11] R. Fu, Y. Yan, C. Roberts, Z. Liu, Y. Chen, The role of dipole interactions in hyperthermia heating colloidal clusters of densely-packed superparamagnetic nanoparticles, Sci. Rep. 8 (2018) 4704. https://www.nature.com/articles/s41598-018-23225-5.
[12] A.F. Abu-Bakr, A.Y. Zubarev, On the theory of magnetic hyperthermia: clusterization of nanoparticles, Phil. Trans. R. Soc. *A* 378 (2171) (2020) 20190251, https://doi.org/10.1098/rsta.2019.0251.
[13] K. Simeonidis, M.P. Morales, M. Marciello, M. Angelakeris, P. de la Presa, A. Lazaro-Carrillo, A. Tabero, A. Villanueva, O. Chubykalo-Fesenko, D. Serantes, In-situ particles reorientation during magnetic hyperthermia application: shape matters twice, Sci. Rep. 6 (2016) 38382, https://doi.org/10.1038/srep38382.
[14] E. Myrovali, N. Maniotis, A. Makridis, A. Terzopoulou, V. Ntomprougkidis, K. Simeonidis, D. Sakellari, O. Kalogirou, T. Samaras, R. Salikhov, M. Spasova, M. Farle, U. Wiedwald, M. Angelakeris, Arrangement at the nanoscale: effect on magnetic particle hyperthermia, Sci. Rep. 6 (2016) 37934, https://doi.org/10.1038/srep37934.
[15] G. Cordova, B.Y. Lee, Z. Leonenko, Magnetic force microscopy for nanoparticle characterization, Nano World J. 2 (1) (2016) 10–14. https://doi.org/10.17756/nwj.2016-022.
[16] H. Lai, F. Xu, L.I. Wang, A review of the preparation and application of magnetic nanoparticles for surface-enhanced Raman scattering, J. Mater. Sci. 53 (12) (2018) 8677–8698, https://doi.org/10.1007/s10853-018-2095-9.
[17] L. Harasztosi, D.L. Beke, Acta Physica Debrecenia 30 (1995) 7.
[18] N. K. Howell, G. Arteaga, S. Nakai, E. C. Y. Li-Chan, Raman Spectral Analysis in the C-H Stretching Region of Proteins and Amino Acids for Investigation of Hydrophobic Interactions J. Agric. Food Chem. 1999 47 1999 924 933 10.1021/jf981074l.
[19] N. Mironova-Ulmane, A. Kuzmin, I. Sildos, Ma. Pärs, Polarisation dependent Raman study of single-crystal nickel oxide, Centr. Eur. J. Phys., 1096-1099 (2011), https://doi.org/10.2478/s11534-010-0130-9.
[20] N. Mironova-Ulmane, A. Kuzmin, I. Steins, J. Grabis, I. Sildos, M. Pärs, Raman scattering in nanosized nickel oxide NiO, J. Phys. Conf. Ser. 93 (2007) 012039, https://doi.org/10.1088/1742-6596/93/1/012039.
[21] N. Mironova-Ulmane, A. Kuzmin, J. Grabis, I. Sildos, V.I. Voronin, I.F. Berger, V. A. Kazantsev, Structural and magnetic properties of nickel oxide nanopowders, Solid State Phenom. 168–169 (2011) 341–344, https://doi.org/10.4028/www.scientific.net/SSP.168-169.341.
[22] A.M. Jubb, H.C. Allen, Vibrational spectroscopic characterization of hematite, maghemite, and magnetite thin films produced by vapor deposition, ACS Appl. Mater. Interfaces 2 (10) (2010) 2804–2812, https://doi.org/10.1021/am1004943.
[23] M. Hanesch, Raman spectroscopy of iron oxides and (oxy)hydroxides at low laser power and possible applications in environmental magnetic studies, Geophys. J. Int. 177 (2009) 941–948, https://doi.org/10.1111/j.1365-246X.2009.04122.x.
[24] D.L.A. de Faria, S. Venâncio Silva, M.T. de Oliveira, Raman microspectroscopy of some iron oxides and oxyhydroxides, J. Raman Spectrosc. 28 (1997) 873–878, https://doi.org/10.1002/(SICI)1097-4555(199711)28:11%3C873::AID-JRS177%3E3.0.CO;2-B.
[25] A.V. Mikhonin, N.S. Myshakina, S.V. Bykov, S.A. Asher, UV resonance raman determination of polyproline II, extended 2.51-helix, and β-sheet Ψ angle energy landscape in poly-L-lysine and poly-L-glutamic acid, J. Am. Chem. Soc. 127 (2005) 7712–7720, https://doi.org/10.1021/ja044636s.
[26] D. Carrier, M. Pezolet, Raman spectroscopic study of the interaction of poly-L-lysine with dipalmitoylphosphatidylglycerol bilayers, Biophys J. 46(4): 497–506 (1984), https://dx.doi.org/10.1016%2FS0006-3495(84)84047-3.
[27] L. Ma, Z. Ahmed, A.V. Mikhonin, S.A. Asher, UV resonance Raman measurements of poly-L-lysine's conformational energy landscapes: dependence on perchlorate concentration and temperature, J. Phys. Chem. B 111 (2007) 7675–7680, https://doi.org/10.1021/jp0703758.
[28] P. Bender, J. Fock, M.F. Hansen, L.K. Bogart, P. Southern, F. Ludwig, F. Wiekhorst, W. Szczerba, L.J. Zeng, D. Heinke, N. Gehrke, M.T. Fernández Díaz, D. González-Alonso, J.I. Espeso, J. Rodríguez Fernández, C. Johansson, Influence of clustering on the magnetic properties and hyperthermia performance of iron oxide nanoparticles, Nanotechnology 29 (42) (2018) 425705, https://doi.org/10.1088/1361-6528/aad67d.
[29] M. Angelakeris, Magnetic nanoparticles: a multifunctional vehicle for modern theranostics, BBA 1861 (6) (2017) 1642–1651, https://doi.org/10.1016/j.bbagen.2017.02.022.